Salt Damage and Electrical Leak on Porous Walls: A Simulation Study

Supti Sadhukhan[1], Tapati Dutta[2,3*]

[1]*Department of Physics, Jogesh Chandra Chaudhuri College, Kolkatata-700033, India.*

[2*]*Physics Department, St. Xavier's College, Kolkata-700016, India.*

[3*]*Condensed Matter Physics Research Centre, Physics Department, Jadavpur University, Kolkata-700032, India.*

Abstract:
Salt damage to materials is a challenge faced by both industry and the common man causing great economic losses. Two aspects of salt damage are addressed in this work- (i) salt crystallization on exposed porous wall (ii) salt damage induced electrical leakage in the damp porous wall. We address salt damage to porous wall where damage is caused by the deposition of saline droplets of water on the surface, as in salt spray, using a 3-dimensional modelling of the entire phenomena – construction of a porous system - deposition and drying of salt-spray - salt crystallization and finally electrical leakage. The two problems are studied as a function of different drying rates . Our studies indicate that electrical leakage due to salt damp on walls shows a damped oscillatory behaviour. The frequency of oscillation is higher for higher drying rates. The authors explain the oscillation in the electrical output as a competition between two time scales - (a) diffusive transport of salt ions (b) increase in salt concentration in exposed pores at channel surface that is determined by the drying rate.

Keywords: Salt damage; Porous material; Simulation; Crystallization; Electrical leakage

1. INTRODUCTION

Salt-induced damage poses a grave threat to numerous buildings worldwide, specially historical buildings and archaeological sites [1, 2, 3, 4, 5, 6, 7, 8]. Temperature fluctuations, wind and water erosion, changes in relative humidity can cause salt induced damage to porous walls with both chemical and physical consequences. The different mechanisms of salt damage involve: (i) Salt crystals growth within pores and cracks of building materials that exert pressure that can eventually lead to surface cracks; (ii) Repeated cycles of salt dissol-lution and re-crystallization can cause progressive weakening and loss of material over time; (iii) Absorbing moisture by salts can cause swelling and deterioration; (iv) Weathering of surfaces can occur due to chemical reaction between absorbed salts and building materials. Salt deposition on porous walls can occur from chemical reaction due to acidic rain [9], rising damp [10], sea spray [11] to name a few sources. Usually sulfates, sulfites, nitrates, and nitrites occur through urban pollution deposits; nitrates can form through bird excreta; whereas chlorides trace their origins to sea-spray, flooding and rising damps [12, 13]. Upon deposition on porous walls, salts can effectively decrease the pore sizes thereby increasing capillary suction of the walls [14], enhance the hygroscopic property of the wall [15] and even affect the drying properties of walls [16, 17]. The saturated vapour pressure of water being higher than salt water, the drying rate of water saturated bricks is reported to be higher than bricks saturated with salt water. Salt crystallization, often referred to as salt damage manifests itself through efflorescence, surface flaking, granular degeneration or alveolarization (honeycomb weathering). Super-saturated saline water can easily deposit salt in materials with large internal surface area [18, 19], especially during evaporation of moisture. Crystallization is facilitated in smaller pores as they can better maintain the state of supersaturation [20] but are affected by pore structure, solution properties such as viscosity and surface tension, type of salt, temperature and relative humidity as well [21]. Following the earliest work of Correns [22], various approaches have been proposed to calculate crystalline pressure [23, 24, 25, 26, 27, 28, 29] factoring the role of solute activity [30], crystal curvature [31] and the chemical potential of crystal facets. In evaporative crys-tallization processes, crystals precipitate at the drying front where the water evaporates and hence, the solution concentration increases up to super-saturation.

*Address correspondence to this author at the Department of Physics, St. Xavier's College, Kolkata-700016, India; E-mail: tapati_mithu@yahoo.com

E-ISSN: 2410-1869/19

Efflorescence occurs when the liquid flow within the pores is sufficient to meet reach and evaporate on the outer surface of the evaporative flux, allowing the moisture to material. In contrast, subflorescence happens when the liquid flow is inadequate to meet this demand, resulting in the drying front being located inside the material. This internal drying process along with the gradual slowing of solution transport within the pores, typically results in a drop in temperature as water evaporates and supersaturation increases.

In this work we concentrate on salt damage on porous walls caused by the deposition of salt water spray. We consider a situation where salt spray on porous walls evaporate at a rate *r* determined by ambient conditions of temperature and relative humidity. Upon evaporation, the residual salt is deposited on the pore wall. It is assumed that the pore walls are already damp and hence have a surface layer of moisture lining them, or that the pores already contain water that has penetrated to a certain depth from the surface layer depending on the velocity of spray, pore size and shape and properties of surface tension and viscosity. In either situation, the residue salt increases the salinity at the pore surface layers. If the increase in salt concentration causes supersaturation at the pore, crystallization of salt can occur on the pore wall. This can result is partial clogging of the pore. At the same time, an increase in salinity at the pore site can result in diffusion of salt through connected pore spaces that are filled with water. The competition between the drying rate and the diffusion of salt (from regions of high to low concentration) through connected pore spaces determine the final evolution of salt crystallization on the porous wall. We investigate the extent of salt crystallization due to evaporation of salt spray deposition on porous walls.

There is another consequence of salt damage that we investigate in this work - capillary transport of saline water driven by potential pressure gradient from the exposed surface to the receding wetting front by the process of diffusion. This diffusion is a function of the permeability of the material [32, 33], its porosity and initial degree of saturation; the boundary conditions of flow are determined by the pore size distribution, surface tension of the fluid and the contact angle with the matrix. As a result of the inward penetration of saline water into the porous matrix, the initial dry porous channels transform to electrical conducting pathways. Hence any voltage difference across the moisture laden conduits of saline water act can as paths of short circuit electric leaks - a common occurrence in damp walls. Thus changes in dielectric constant and bulk electrical conductivity are a measure of the extent of solute penetration in the capillary channels due to moisture imbibition.

In the following sections we describe in sequence : (i) generation of a 3-dimensional porous structure using a Relaxed Bidisperse Ballistic Deposition (RBBDM) model [34] of variable porosity; (ii) Model the deposition of salt spray on the exposed surface of the pore-matrix ensemble as a function of the ambient conditions (iii) Simulate evaporation of moisture from the exposed surface and consequent deposition of solute residue on pore wall (iv) Enable diffusive flow through connected channel in the porous matrix through pore channels that are completely damp and finally (v) Estimate the bulk electrical conductivity of the porous media as a measure of possible electrical leak.

2. MATERIALS AND METHODS

The first step is the generation of the 3-dimensional porous matrix using the RBBDM. Next, the entire porous wall is exposed to salt spray. Drying rate controls the crystal formation in the pores. TDRW is employed for transport of walkers mimicking the ions of the solution. A measure of the electrical conductivity is estimated from the number of walkers arriving at the bottom of the sample.

2.1 RBBDM

The ‘RBBDM’ has the potential of generating a structure with a connected rock phase that is needed for any stable structure, and a ‘tunable porosity’. The details of RBBDM have been discussed in earlier works [35, 36, 37] in order to study various transport properties like permeability and conductivity through sedimentary rocks. A brief outline of the model will be given here. The basic algorithm is to deposit particles of two different sizes ballistically. In three dimensions (*2 + 1* model), we drop square *1×1×1* and elongated *2×1×1* grains on a square substrate. The longer grains deposit with their long axis parallel to the bedding plane and along either of the two transverse directions with equal probability. The

cubic grains are chosen with a probability p and elongated grains with probability $1 - p$. The porosity ϕ, defined as the vacant fraction of the total volume, depends on the value of p. For $p = 1$, a dense structure with no pores is produced. As the fraction of longer grains is increased, unstable overhangs can develop. If a larger particle settles on a smaller particle, a one-step overhang is created. If a second larger particle settles midway on the previous large particle, a two-step overhang is created if there is no supporting particle immediately below the protrusion of the second overhang. A two-step overhang created in this way, is not stable and the second large particle topples over if possible, according to the rule scheme as shown in Figure (1a) leading to compaction. Here a $L_x \times L_x \times L_z$ size sample was generated, from which a $L_x \times L_x \times L_{z'}$ sample was selected after the porosity had stabilized to within 0.001%. The sample of size $50 \times 50 \times 10$ selected for study, was chosen far below the surface to eliminate surface effects. The pore clusters have an elongated and interconnected appearance along the direction of grain deposition (z-direction) while the distribution of pores along the

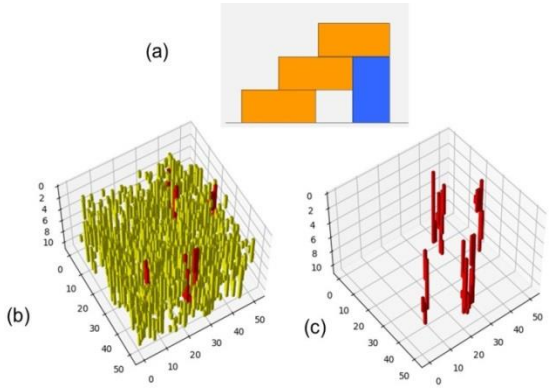

Figure 1: (a) Schematic of toppling of grains to lower potential energy states. (b) Pore clusters in 3D-sample marked in yellow. (c) Connected pore channels spanning the sample indicated in red.

transverse plane is homogeneous. As the fraction of larger grains is decreased, the porosity of the sample decreases and the pore distribution becomes more anisotropic nature. The Hoshen-Kopelman algorithm [38] was then run on the porous sample to identify structure spanning pore channels which are essential to study electrical conductivity.

2.2 Absorption of salt spray and salt crystallization

The model assumes that the entire porous wall is exposed to salt spray and is therefore covered uniformly by droplets of salt water. The evaporation probability of the droplets from the wall is dependent on ambient conditions and is implemented in our model by the parameter r. Simply put, a higher r value would imply higher evaporation probability and vice-versa.

To implement evaporation of water from the droplets, a fraction r of the total pores on the surface is chosen randomly that will lose water due to evaporation. The salinity of the salt-spray is uniform and taken to be C_0. When a pore cell loses water due to evaporation, the salt concentration inside the cell, increases. If the concentration becomes greater than the critical concentration Ccr required for crystallization, a unit of salt crystal is deposited on the pore wall. Since a single unit of salt crystal is much smaller than a pore size, we envisage a unit pore as divided into M units of micro-pores. Q number of walkers are required to form crystals to clog a micro-pore. If $M^*(t)$ is the number of micro-pores clogged at any instant t such that $0 < M^*(t) < M$, the pore is said to be partially clogged. It may be remembered that every crystallization event decreases the concentration of salt in the solution of the pore cell.

In our model the salt units are mimicked by random walkers. The increase in the salt concentration of a completely unclogged pore cell that loses water by evaporation is mimicked by introducing $n(t)$ number of random walkers at a timestep t where

$$n(t)=C_0(M-M^*(t)) \quad (1)$$

Here C_0 is the initial salinity of a spray drop;
$M - M^*(t)$ is the number of unclogged micro-pores in a single pore unit. If the salinity (i.e. the number of random walkers) in a pore unit is greater than the critical salt saturation (critical number of random walkers), salt crystals will precipitate. This condition is therefore summarized as

$$C(t)-Ccr = \delta C(t) \geq 0 \quad (2)$$

$C(t)$ is the salt concentration in a pore cell at any instant of time t and Ccr is the critical concentration. If the condition given by Eq.(2) is satisfied, $\delta C(t)$ goes into the creation of micro-crystals that nucleate on the pore unit wall. The number of micro-pores that get clogged at any time step per unit pore cell is

$$M^*(t)=\delta C(t)/Q \quad (3)$$

In other words once the critical salinity is achieved it is held constant as the excess $\delta C(t)$ is precipitated as micro-crystals - the phenomena mimicked in our model by removing

$$n_{kill}=\delta C(t) \quad (4)$$

number of random walkers from the pore unit. Thus only $M - M^*(t)$ of the original pore unit now remains unclogged and act as entry points to saline spray. Evaporation from an exposed pore is allowed as long as the pore is not completely clogged.

2.3 Transport mechanism in pore channels

The pore channels often have a layer of moisture on the walls and are fluid filled; being either completely filled with water vapour or partially filled with water and vapour. The random walkers that do not contribute to salt crystallization on the walls get transported in the pore, conduits by diffusion following the salt gradients in the channel. It may be expected that the salt concentration is higher at the exposed face on the wall surface than further deep down. We incorporate diffusion of salt ions by the Time Domain Random Walk (TDRW) mechanism, in which random walkers mimic the ions. To facilitate the transport mechanism the pore channel is discretized by overlaying a 3-D grid mesh of cubes having size $\delta x = \delta y = \delta z = 5 \times 10^{-5}\ m$.

Though we do not introduce any explicit advective velocity, the pore channels remain filled with moisture due to evaporative pull exerted on the surface of the channel. In our model we consider diffusion as the only mechanism by which walkers transport within the system. The time of transition taken by a walker to jump from one pore grid to another is dependent on the local velocity, whereas the distance covered in one jump is fixed. The approach discussed by [39,40] is extensively utilized where the probability of transition to the adjacent pixel (grid) and the associated time duration for the jump is derived from the Advection-Dispersion Equation.

$$\frac{\partial \mathrm{C}}{\partial \mathrm{t}} + \nabla.(\mathbf{V}\mathrm{C}) - \nabla.\mathrm{D}\,\nabla\mathrm{C} = 0 \quad (5)$$

where the symbols having their usual meanings. discretization of Eq.(5) in 3-D yields

$$\frac{\partial \mathrm{C_i}}{\partial \mathrm{t}} = -\frac{\mathrm{u}}{\mathrm{h}}\left[\mathrm{C_i} - \mathrm{C_{up_x}}\right] - \frac{\mathrm{v}}{\mathrm{h}}\left[\mathrm{C_i} - \mathrm{C_{up_y}}\right] - \frac{\mathrm{w}}{\mathrm{h}}\left[\mathrm{C_i} - \mathrm{C_{up_z}}\right] + \frac{\mathrm{D}}{\mathrm{h^2}}\left[\mathrm{C_{dn_x}} + \mathrm{C_{up_x}} - 2\mathrm{C_i}\right] + \frac{\mathrm{D}}{\mathrm{h^2}}\left[\mathrm{C_{dn_y}} + \mathrm{C_{up_y}} - 2\mathrm{C_i}\right] + \frac{\mathrm{D}}{\mathrm{h^2}}\left[\mathrm{C_{dn_z}} + \mathrm{C_{up_z}} - 2\mathrm{C_i}\right] \quad (6)$$

where $\mathrm{C_i}$ is the concentration at the ith pixel. The terms $\mathrm{C_{up_x}}$ and $\mathrm{C_{dn_x}}$ denote the concentration values at the pixels adjacent to i along x axis, with $\mathrm{C_{up_x}}$ indicating a higher concentration (up≡upstream), and $\mathrm{C_{dn_x}}$ corresponding to a lower concentration (dn ≡downstream) compared to $\mathrm{C_i}$. Similarly, the notations $\mathrm{C_{up_y}}$ and $\mathrm{C_{dn_y}}$, and $\mathrm{C_{up_z}}$ and $\mathrm{C_{dn_z}}$ convey analogous meanings along the y-axis and z-axis respectively. The distance between two adjacent pixels is represented by h while u, v and w are the resolved components of **V** along the *x, y* and *z*- axes respectively.

The generalized form of Eq.(6) is

$$\frac{\partial \mathrm{C_i}}{\partial \mathrm{t}} = -\mathrm{C_i}\sum_j \mathrm{b_{j,i}} + \sum_j \mathrm{C_j}\,\mathrm{b_{i,j}} \quad (7)$$

where,

$$\mathrm{b_{up_x,i}} = \mathrm{b_{up_y,i}} = \mathrm{b_{up_z,i}} = \mathrm{b_{i,dn_x}} = \mathrm{b_{i,dn_y}} = \mathrm{b_{i,dn_z}} = \frac{\mathrm{D}}{\mathrm{h^2}}$$

$$\mathrm{b_{dn_x,i}} = \mathrm{b_{i,up_x}} = \frac{\mathrm{D}}{\mathrm{h^2}} + \frac{\mathrm{u}}{\mathrm{h}}$$

$$\mathrm{b_{dn_y,i}} = \mathrm{b_{i,up_y}} = \frac{\mathrm{D}}{\mathrm{h^2}} + \frac{\mathrm{v}}{\mathrm{h}}$$

$$\mathrm{b_{dn_z,i}} = \mathrm{b_{i,up_z}} = \frac{\mathrm{D}}{\mathrm{h^2}} + \frac{\mathrm{w}}{\mathrm{h}}$$

Walkers originating from the same position may traverse different trajectories and distances within the same time of observation depending on the b_{ij} of each successive pore cell they encounter. The b_{ij} encapsulate the effective velocities in the six directions accessible to a walker from the residing pore cell. The transition probability between two adjacent pixels, from j to i, and the time duration involved are presented respectively as [38, 39]

$$\mathrm{W_{ij}} = \frac{\mathrm{b_{ij}}}{\sum_j \mathrm{b_{ij}}} \quad (8)$$

$$\mathrm{T_j} = \frac{1}{\sum_j \mathrm{b_{ij}}} \quad (9)$$

In the absence of advective velocities, i.e $u = v = w = 0$, all walkers have equal $\mathrm{T_j}$, say τ. Taking $h = 5 \times 10^{-5} m$, $D = 25 \times 10^{-10}\ m^2/s$, we calculate $T_j = 1/6\ s$ for j running from 1 to 6 in 3D.

The mobility of different ions may be different as per their size. Higher the mobility, lesser is the time of residence of an ion in a given pore pixel. In this system we have kept the simple assumption of all the ions being identical in size and therefore of equal mobility. This implies that the transition time of the ions is identical too. The walkers are allowed to diffuse for time τ . If the neighbouring cell is a matrix

cell, they reside in the same pore. Also movement above the topmost layer is restricted as walkers are not allowed to exit the system from this end. Any walker who has reached the bottom most layer has a probability of exiting the system.

2.4 Electrical conductivity

Electrical conductivity in brine filled pore channels of sedimentary rocks using finite difference schemes have been discussed at length in previous works by the author [34]. We estimate the measure of electrical leakage in salt damaged porous walls as proportional to the cumulative sum of all random walkers (ions) that finally reach the bottom layer of the channels, W_{bottom}. Once a channel entry point is fully clogged, it stops acting as a conducting path for electricity.

3. RESULTS AND DISCUSSION

The disordered porous system was generated using the RBBDM with p = 0.95, which means large particles of size 2 × 1 × 1 have probability 1-p = 0.05 and the porosity of the sample is 0.098. All pore clusters were identified as indicated in Figure (1b) with system spanning clusters marked separately by red, Figure (1c). It is apparent that porosity shows anisotropy along the direction of grain deposition with pore clusters having an elongated appearance. With increasing time steps, there is greater probability of evaporation of droplets from any pore site. Thus for a fixed drying rate *r*, as we move along any row of Figure (2), the pores gradually turn from green to red as time progresses. The green colour indicates completely unclogged pores, yellow indicates partially clogged pores and red indicates pores that are completely clogged. If we move down the columns of Figure (2), the transition from green to red happens faster as the drying rate increases. Figure (3) shows that the cumulative number of clogged pores follow a sigmoid variation with simulation time steps. The cumulative maximum of pores is reached quicker for higher evaporation rates as expected. This result displays the dependence of salt damage on porous walls as a function of drying rate.

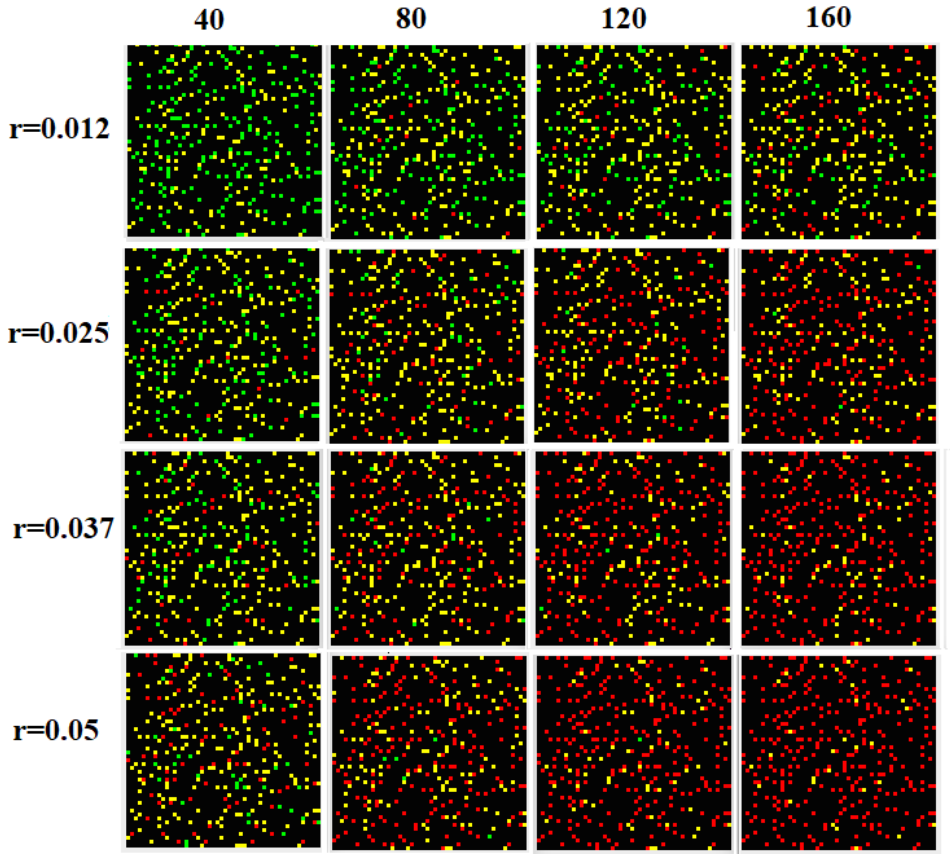

Figure 2: A matrix figure showing screenshots of the top surface of the sample at different time steps of simulation for different evaporation rates *r*. The timesteps of *40, 80, 120,* and *150* are indicated on the column heads; the rows correspond to different evaporation rates *r*. Green colours indicate open pores, yellow pores

indicate partially clogged pores and red colour indicated totally clogged pores respectively.

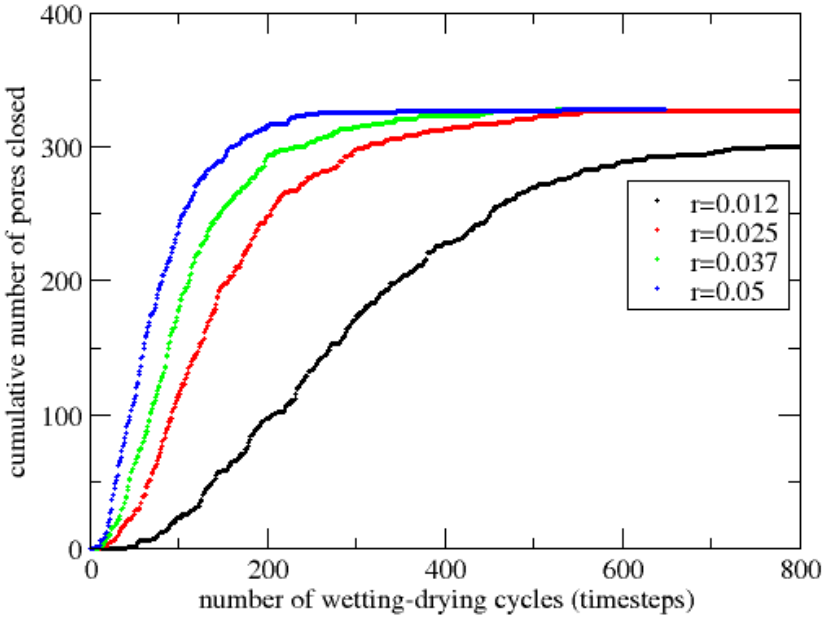

Figure 3: Variation of cumulative number of clogged pores on sample surface with simulation timesteps for different drying rates *r*.

The electrical leakage in salt damaged porous wall is estimated by counting the number of walkers who have traversed the length of the sample to reach the bottom layer of the walkers. Therefore while considering electrical leakage we concentrate only on pore channels that span the wall width. If during the process of drying and salt precipitation, the channel entry point gets completely clogged by salt, it ceases to act as a conducting ion path. In Figure (4 a-d) we display the rate of cumulative micro-pore closure of only the wall width spanning pore channels for different drying rates. In Figure (4 e-h) we have displayed the number of walkers in the last layer with time for the corresponding drying rates as we expected a correlation between the two processes;

The first point noted is that a faster drying rate r results in a quicker clogging of the pores exposed on the wall surface, Figure (2). Consequently, the transport of salt ions in the wall's pore channels stops earlier with decreasing value of *r*, causing the graphs to saturate as in Figure (4 a-d). This is also manifested in the very low number of random walkers (ions) that can travel through the channel (Figure 4e-h), i.e. the electrical conductivity of the walls due to saline water damp ceases earliest for the highest *r*. Thus higher drying rate will cause electrical leak only as long as transport can occur through the channels; a slower drying rate is responsible for greater electrical leakage as the complete closure of exposed pores due to salt crystallization takes a longer time.

Figure.(4e-h) shows oscillations in the number of walkers that exit the pore channels with time. There is an inherent competition between two time scales in the entire process - (i) the time of travel from entry to exit pore of a pore channel by the random walkers that is controlled by the concentration gradient (ii) time taken to replenish random walkers at the channel entry point which is determined by drying rate r and the unit pore size *M*. As long as the latter is greater than the former, an output of walkers is obtained at the channel exit, i.e. the porous wall is conducting. However if the replenishment of random walkers at the entry points is slower than the rate of transport through the channel, the output at the exit points can decrease even to zero as is seen in Figure (4f-h). As the number of random walkers again builds up at the entry points of the channels, electrical conductivity gradually increases again. A close examination of the cumulative clogging rate of micro-pores and their corresponding electrical leakage for any drying rate *r*, shows that when the former graphs reach a plateau, there is a spike in the number of random walkers that traverse the length of the pore channels contributing to electrical leakage. For slower drying rates, Figure (4a), pores clog gradually. This ensures that though there are fluctuations, there are sufficient number of random walkers that can conduct electricity for a longer time, Figure (4e).

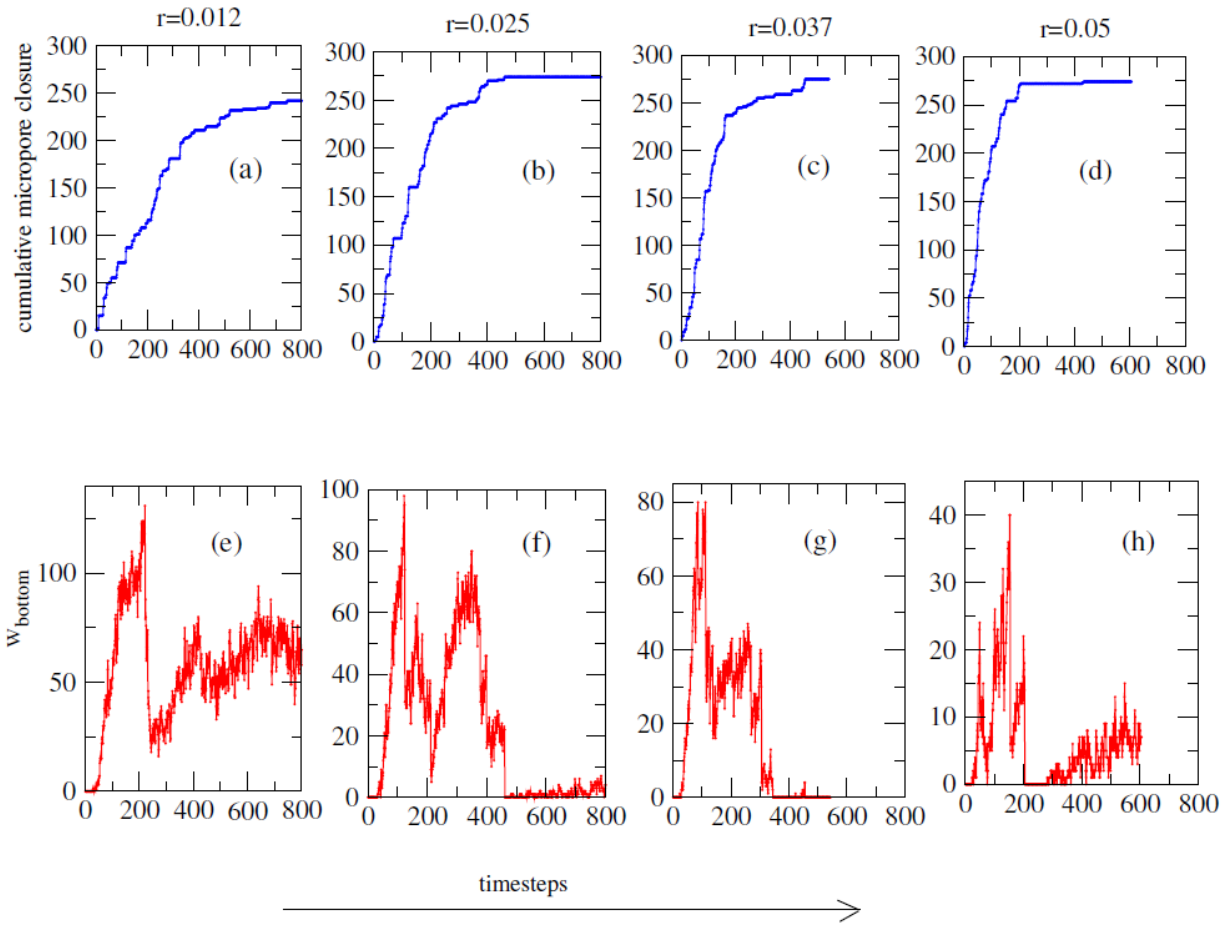

Figure 4: First row of sub-figures display the cumulative micro-pore closure of pore channels spanning the wall width versus time for drying rates *(a) r = 0.012 (b) r = 0.025 (c) r = 0.037 (d) r = 0.05*; the second row of sub-figures display the cumulative number of random walkers (ions) in the bottom layer of sample as a function of time steps for identical and corresponding drying rates.

4. CONCLUSIONS

The phenomenon of salt damage on porous walls and consequent electrical leakage through them has been examined through a simulation model in this work. The authors have generated a 3-dimensional disordered porous wall where the matrix is a completely connected phase. It is however possible that all the pores may not be interconnected, but there exist some system spanning pore channels in the structure. In this structure salt spray deposits uniformly as droplets of saline water on the surface exposed to the environment. The effect of salt crystallization on the exposed wall is dependent on the parameter *r*. The extent of salt crystallization on the exposed wall surface has been found to be a sigmoidal function of time for all evaporation rates. The higher the evaporation rate the steeper is the slope of the curves but in the asymptotic limit they reach the value of the total number of exposed pores.

The other important aspect of this work is the study of electrical leakage through the salt ions that remain in the moisture laden pore channels that span the wall widths. Using TDRW on a discretized spanning pore channel, electrical conductivity was estimated as a function of time. The salt ions that move diffusively through the channels are carriers of electricity. It was observed that lower drying rates enabled electrical leakage to continue over longer time spans. More interestingly, the electrical conduction showed almost periodic fluctuation in their outputs, the frequency of fluctuation appeared to increase with increasing drying rates. For a constant drying rate, there is a general trend of the amplitude of the fluctuation to decrease with time. The authors explain the oscillatory nature of the leakage current as due to a competition between two rates- (i) the rate of diffusive transport of ions through the channels that is guided by the salt concentration gradient between the inlet and exit of the pore channel, (ii) to the rate at which salt ions seep into

the pores on the exposed surface. The latter process is not only a function of the drying
rate itself but also a function of the extent of salt clogging the exposed pores.

This is a simple model of salt damage which has not factored the role of surface tension in the penetration of saline water in the pore space. This would require a consideration of pore size and shape and their distribution to be known. Further complexities like 3-dimensional salt build-up on the exposed wall has not been considered in this work. The authors hope to report these effects on salt damage in future communication.

REFERENCES

[1] Goudie A, Viles HA. Salt Weathering Hazard. Chichester, UK: Wiley 1997.ISBN 9780471958420.

[2] Lewin SZ. The Mechanism of Masonry Decay Through Crystallization. In Conservation of Historic Stone Buildings and Monuments; Committee on Conservation of Historic Stone Buildings and Monuments; National Materials Advisory Board; Commission on Engineering and Technical Systems; Division on Engineering and Physical Sciences; National Research Council, Ed.; National Academies Press: Washington, DC, USA, 1982; p. 120–144. ISBN 978-0-309-03275-9.

[3] Rodriguez-Navarro C, Doehne E. Salt weathering: Influence of evaporation rate, supersaturation and crystallization pattern. Earth Surf Process Landforms 1999; 24: 191-209.

[4] Charola AE. Salts in the Deterioration of Porous Materials: An Overview. J Am Inst Conserv 2000; 39: 327-343.

[5] Harris SY. Building Pathology: Deterioration, Diagnostics, and Intervention; Wiley: New York, NY, USA, 2001; ISBN 9780471331728.

[6] Doehne E. Salt weathering: A selective review. In Natural Stone,Weathering Phenomena, Conservation Strategies and Case Studies; Siegesmund S, Weiss T, Vollbrecht A, Eds; Geological Society of London: London, UK, 2002; 205, pp. 51-64. ISBN 9781862394537.

[7] Lubelli B, van Hees RPJ, Groot CJWP. The role of sea salts in the occurrence of different damage mechanisms and decay patterns on brick masonry. Constr Build Mater 2004; 18:119-124.

[8] Bersani D, Madariaga JM. Applications of Raman spectroscopy in art and archaeology. J Raman Spectrosc 2012; 43:1523-1528.

[9] Warscheid T and Braams J. Biodeterioration of stone: a review. International Biodeterioration & Biodegradation 2000; 46:343-368.

[10] Doehne E and Price C. Stone Conservation: An Overview of Current Research. 2nd ed. The Getty Conservation Institute, Los Angeles, Calif, USA; 2010.

[11] Charola AE. Salts in the deterioration of porous materials: an overview. Journal of the American Institute for Conservation 2013; 39:327-343.

[12] Hall C and Hoff W. Liquidmovements. Materials World 2007; 15:24-26.

[13] Zappia G, Sabbioni C, Riontino C, Gobbi G and Favoni O. Exposure tests of building materials in urban atmosphere. Science of the Total Environment 1998; 224: 235-244.

[14] Lubelli B, VanHees R PJ, Brocken HJP. Experimental research on hygroscopic behaviour of porous specimens contaminated with salts. Construction and Building Materials 2004; 18:339-348.

[15] Koniorczyk M and Wojciechowski M. Influence of salt on desorption isotherm and hygral state of cement mortar—modelling using neural networks. Construction and Building Materials 2009; 23:2988-2996.

[16] Voronina V, Pel L, Kopinga K. Effect of osmotic pressure on salt extraction by a poultice. Construction and Building Materials 2014; 53:432-438.

[17] Gupta S, Huinink HP, Prat M, Pel L, Kopinga K. Paradoxical drying of a fired-clay brick due to salt crystallization. Chemical Engineering Science, 2014; 109:204-211.

[18] Collepardi M. Degradation and restoration of masonry walls of historical Buildings . Materials and Structures 1990; 23: 81-102.

[19] Rovnaníková P. Environmental pollution effects on other building materials, in Environmental Deterioration of Materials, A. Moncmanov´a, Ed., pp. 217-248, WIT Press, Southampton, UK, 2007.

[20] Benavente D, Garc´ıa del Cura MA, Garc´ıa-Guinea J, S´anchez-Moral S, Ord´o˜nez S. Role of pore structure in salt crystallisation in unsaturated porous stone. Journal of Crystal Growth 2004; 260: 532-544.

[21] Doehne E. Salt weathering: a selective review. Geological Society Special Publication 2002; 205: 51-64.

[22] Correns CW. Growth and dissolution of crystals under linear pressure. Discuss. Faraday Soc. 1949; 5: 267.

[23] Steiger M. Crystal growth in porous materials—I: The crystallization pressure of large crystals. J Cryst Growth 2005; 282: 455-469.

[24] Benavente D, Garc´ıa Del Cura MA, Fort R, Ord´o˜nez S. Thermodynamic modelling of changes induced by salt pressure crystallization in porous media of stone. J. Cryst. Growth 1999; 204: 168-178.

[25] Min D, Mingshu T. Formation and expansion of ettringite crystals. Cem Concr Res 1994; 24: 119-126.

[26] Desarnaud J, Bonn D, Shahidzadeh, N. The Pressure .induced by salt crystallization in confinement. Sci Rep 2016; 6:1-8.

[27] Sekine K, Hayashi K. In situ observation of the crystallization pressure induced by halite crystal growth in a microfluidic channel. Am Mineral 2011; 96: 1012-1019.

[28] Hamilton A, Koutsos V, Hall C. Direct measurement of salt-mineral repulsion using atomic force microscopy. Chem Commun 2010; 46: 5235-5237

[29] Pitzer KS, Kenneth S. Activity Coefficients in Electrolyte Solutions. CRC: Boca Raton, FL, USA, 1991. ISBN 9781351069472. Probl. Chalk 1973; 143: 223-245.

[30] Neugebauer J. The diagenetic problem of chalk. Diagenetic Probl. Chalk 1973; 143: 223–245.

[31] Everett DH. The thermodynamics of frost damage to porous solids. Trans Faraday Soc 1961; 57: 1541-1551.

[32] Culligan PJ, Ivanov V, Germaine JT. Sorptivity and liquid infiltration into dry soil. Adv Water Resour 2005 ; 28:

1010-1020.

[33] Hall C, Hamilton A, Hoff WD, Viles HA, Eklund JA. Moisture dynamics in walls: response to micro-environment and climate change. Proc R Soc A 2011; 467: 194-211.

[34] Sadhukhan S, Dutta T, Tarafdar S. Pore structure and conductivity modelled by bidisperse ballistic in deposition with relaxation. Modelling and Simulation Materials Science and Engineering 2007; 15 (7): 773.

[35] Sadhukhan S, Majumder SR, Mal D, Dutta T, Tarafdar S. Desiccation cracks on different substrates: simulation by a spring network model. Journal of Physics: Condensed Matter 2007;19 (35): 356206.

[36] Sadhukhan S, Dutta T, Tarafdar S. Simulation of diagenesis and permeability variation in two-dimensional rock structure Geophysical Journal International 2007; 169 (3): 1366-1375.

[37] Sadhukhan S, Mal D, Dutta T, Tarafdar S. Permeability variation with fracture dissolution: role of diffusion vs. drift Physica A: Statistical Mechanics and its Applications 2008; 387 (18): 4541-4546.

[38] Hoshen J and Kopelman R. Percolation and cluster distribution. I. Cluster multiple labeling technique and critical concentration algorithm. Phys Rev B 1976; 14:3428.

[39] Dentz M, Gouze P, Russian A, Dweik J, Delay F. Diffusion and trapping in heterogeneous media: an inhomogeneous continuous time random walk approach. Adv Water Resour 2012: 49:13-22.

[40] Sadhukhan S, Dutta T. Existence of convective threshold and its role on temperature in reactive flow through fractured rocks: a simulation study in 2D. J Phys Commun 2018; 2: 045033.

Received on 12-01-2019 Accepted on 14-02-2019 Published on 27-02-2019

DOI: https://doi.org/10.15379/ijmst.v6i2.3737